▌**Magnetic Anisotropy** |*Hot Paper*|

An Experimental and Theoretical Investigation on Pentacoordinated Cobalt(III) Complexes with an Intermediate $S=1$ Spin State: How Halide Ligands Affect their Magnetic Anisotropy

Deborah Brazzolotto,[a] Marcello Gennari,[a] Shengying Yu,[a] Jacques Pécaut,[b] Mathieu Rouzières,[c, d] Rodolphe Clérac,[c, d] Maylis Orio,*[e] and Carole Duboc*[a]

Abstract: Understanding the factors that control the magnitude and symmetry of magnetic anisotropy should facilitate the rational design of mononuclear metal complexes in the quest for single-molecule magnets (SMMs), based on a single metal ion, with high blocking temperatures and large energy barriers. The best strategy is to define magnetostructural correlations through the investigation of a series of metal complexes. It has been demonstrated that the main contribution to the magnetic anisotropy arises from the spin-orbit coupling (SOC) effect in metal-ion-based systems, so current studies focus particularly on the use of both ligands and metal ions possessing a large SOC. In this context, we report a unique series of halide Co^{III} complexes, [CoL(X)], with X = Cl, Br, I (**CoX**) and L = 2,2′-(2,2′-bipyridine-6,6′-diyl)bis(1,1-diphenylethanethiolate), which possess a rare intermediate $S=1$ spin ground state. The $S=1$ Co^{III} complexes are attractive species because they possess a remarkably large axial zero-field splitting (defined by D from the following Hamiltonian: $\boldsymbol{H}=DS_z^2$), as well as the halide ligands inducing large SOC constants. The single-crystal X-ray structures reveal that the **CoBr** and **CoI** complexes are isostructural with the previously described **CoCl** complex. Their coordination sphere displays a distorted pentacoordinated square pyramidal geometry, with the halide located in the Co^{III} axial position. Large positive D values of 35, 26, and 18 cm^{-1} are found for **CoCl**, **CoBr**, and **CoI**, respectively, through analysis of the magnetic susceptibility data as a function of temperature. To rationalize this trend, theoretical calculations based on both density functional theory (DFT) and complete active space self-consistent field (CASSCF) methods are performed successfully. Both the sign and magnitude of D are predicted remarkably well by these theoretical approaches. The DFT calculations also show that the resulting D values originate from a balance of several contributions, and that many factors, including differences in their structural properties and in the contribution of the halide, should be taken into account to explain the trend of D in this series of complexes.

Introduction

A recent strategy to develop single-molecule magnets (SMMs) characterized by high blocking temperatures is to focus on complexes, the magnetic properties of which arise from a single metal ion in a ligand field. These mononuclear systems are mainly based on lanthanides that display the highest blocking temperatures and energy barriers.[1] By contrast, the number of such systems based on transition metal ions is still much more limited, but reasonable energy barriers have been observed, especially for several mononuclear Co^{II} complexes and also for other 3d ions such as a few mononuclear Mn^{III}, Fe^{III}, Fe^{II}, Fe^{I}, and Ni^{I} compounds.[2] This family of systems has been extended recently to the 5d metal ions in the special case of mononuclear Re^{IV} complexes.[3] On the other hand, a recent theoretical investigation has shown that Ni^{II} could be a potentially attractive candidate.[4] This was later confirmed by an experimental study, which reports a Ni^{II} complex displaying field-induced slow magnetic relaxation.[5]

For the rational design of SMMs based on a single metal ion, an important aspect of the current research concerns the identification of the factors governing the sign, symmetry, and magnitude of the magnetic anisotropy in mononuclear complexes.[2a, 6] For the establishment of a correlation between the structure and the zero-field splitting (ZFS) parameters, different series of complexes have been synthesized and characterized by magnetic susceptibility measurements and/or spectroscopic

[a] D. Brazzolotto, Dr. M. Gennari, S. Yu, Dr. C. Duboc
Univ. Grenoble Alpes, DCM, CNRS UMR 5250 38000 Grenoble (France)
E-mail: carole.duboc@ujf-grenoble.fr

[b] Dr. J. Pécaut
Univ. Grenoble Alpes, CEA, INAC-SCIB 38000 Grenoble (France)

[c] M. Rouzières, Dr. R. Clérac
CNRS, CRPP, UPR 8641 F-33600 Pessac (France)

[d] M. Rouzières, Dr. R. Clérac
Univ. Bordeaux, CRPP, UPR 8641 F-33600 Pessac (France)

[e] Dr. M. Orio
Aix Marseille Université, ISM2, CNRS UMR 7313 13397 Marseille (France)
E-mail: maylis.orio@univ-amu.fr

⊞ Supporting information for this article is available on the WWW under http://dx.doi.org/10.1002/chem.201502997.

techniques, with high-field EPR spectroscopy leading to the most accurate data for the determination of the ZFS parameters.[7] In parallel, important theoretical efforts have been made to develop appropriate methodologies to evaluate the ZFS parameters of a given system by determining the physical origin of the magnetic anisotropy, and to compare these theoretical predictions with experimental observations.[8] For such investigations, it is necessary to calculate precisely the two contributions to D, that is, the spin-orbit coupling (D_{SOC}) and the electron–electron spin–spin coupling interaction (D_{SSC}). In line with this approach, DFT calculations have been applied to predict both the sign and magnitude of D, but the magnitude is generally underestimated relative to the experimental data,[9] with the exception of overestimated values in the case of complexes containing heavier halide ligand(s).[10] Other methods, including ab initio approaches, commonly give more satisfactory predictions of D,[9d, 11] but are much more expensive than DFT calculations. It has been concluded from combined experimental and theoretical investigations reported on various transition metal ions, including Mn^{II},[12] Mn^{III},[9d] Ni^{II},[10a, 13] Fe^{II},[14] low-spin Co^{II},[15] and V^{III},[11b] that each case should be treated independently, and no general rule can be applied to determine the most appropriate methodology for the prediction of D. Therefore, for each metal ion, in different oxidation and spin states, systematic studies should be undertaken with a series of benchmark complexes.

It has also been demonstrated that D_{SOC} is the main contribution to the final D value, so particular attention has been given to both ligands and metals characterized by large spin-orbit coupling (SOC). Concerning the ligands, the effect of the SOC contribution of the halide on the magnetic anisotropy has been investigated thoroughly, and it has commonly been observed that the magnitude of D increases from the chloride to the iodide derivatives.[12b, 16]

Regarding the metal ion, whereas the magnetic properties of Co^{II} have received special attention in the last decade,[17] Co^{III} has been remarkably less well studied. It can be found in three different spin states, the singlet being the most popular. Diamagnetic Co^{III} is mainly found in octahedral[18] and tetrahedral geometries,[19] or in tri-[20] and pentacoordinated[21] Co^{III} complexes. The less usual high spin state is found mainly in all types of geometry but in a distorted and/or weak-field environment.[18–21] Interestingly, the Co^{III} complexes with intermediate spin $S = 1$ are found mainly in square planar geometry,[19, 22]

and are attractive because of their remarkably large D magnitudes of up to 145 cm^{-1}.[23] Likewise, a unique distorted trigonal bipyramidal $S = 1$ system displaying a D value of +107 cm^{-1} has also been reported.[24]

Recently, we isolated and characterized a pentacoordinated Co^{III} complex displaying a triplet spin state, that is, the [$Co^{III}L(Cl)$] complex (CoCl) [$L^{2-} = 2,2'$-(2,2'-bipyridine-6,6'-diyl)-bis(1,1-diphenylethanethiolate)], containing an axial chloride ligand.[25] This complex was obtained from the reaction of the dinuclear [$Co^{II}_2(LSSL)$](PF_6)$_2$ (Co$_2$SS^{2+}) in the presence of two equivalents of Et$_4$NCl in CH$_2$Cl$_2$ (Scheme 1). In the present work, following a similar procedure, the corresponding Br and I derivatives are isolated and characterized: [$Co^{III}L(Br)$] (CoBr) and [$Co^{III}L(I)$] (CoI), respectively. Their magnetic properties are determined and compared with those of CoCl. As for CoCl, magnetic measurements also reveal that CoBr and CoI are intermediate $S = 1$ spin systems. Theoretical calculations based on both DFT and CASSCF methods are performed successfully to rationalize the unexpected decrease in D from the chloride to the iodide derivatives.

Results and Discussion

Synthesis and structures

We have recently reported different synthetic methods for the synthesis of CoCl, including a procedure that can be generalized to potentially allow the synthesis of a series of pentacoordinated mononuclear Co^{III} complexes (Scheme 1). The reaction of the dinuclear Co$_2$SS^{2+} complex in the presence of two equivalents of Et$_4$NCl leads to CoCl in good yield.[25] In this reaction, the coordination of one chloride anion on each Co^{II} center in Co$_2$SS^{2+} leads to the reduction of the disulfide bridge and the concomitant oxidation of the Co^{II} ions. Following the same procedure, the addition of two equivalents of Et$_4$NBr and Et$_4$NI to Co$_2$SS^{2+} leads to the formation of [$Co^{III}L(Br)$] (CoBr) and [$Co^{III}L(I)$] (CoI), respectively (Scheme 1).

The X-ray structures of complexes CoBr and CoI (Figure 1 and Table 1) show that both are isostructural with CoCl. In CoBr and CoI, as in the case of CoCl, the N2S2 coordination sphere insured by L^{2-} is completed by the halide anion, leading to a distorted square pyramidal geometry around the Co^{III} ion. The two nitrogen and two sulfur atoms of L^{2-} are located in the equatorial plane, whereas the halide ion occupies the
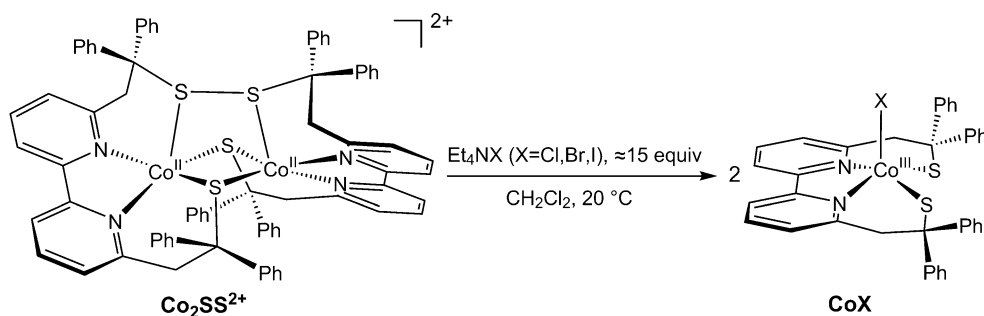
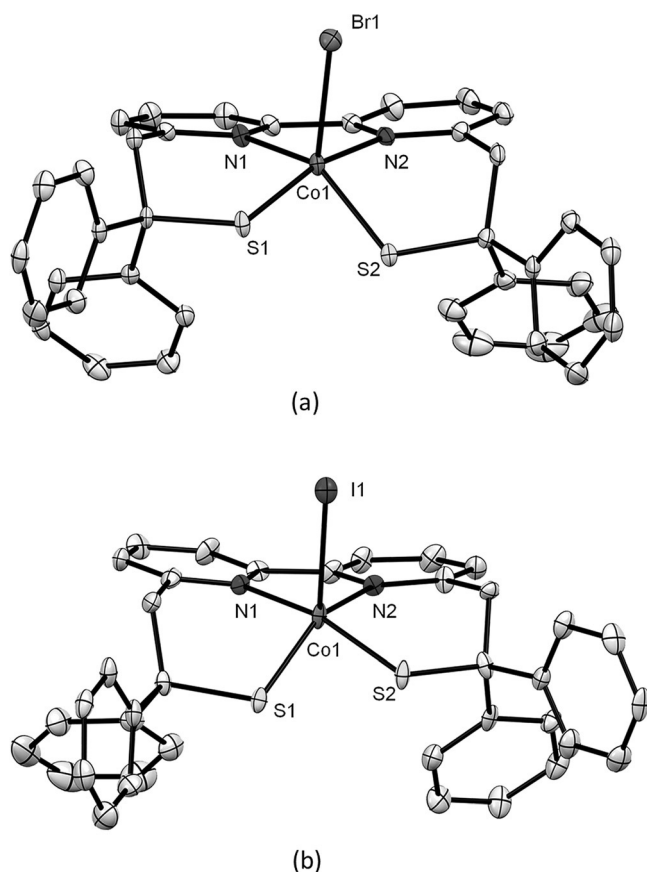**Scheme 1.** Synthesis of CoX (X = Cl, Br, I).

Figure 1. ORTEP-type views of a) **CoBr** and b) **CoI** (thermal ellipsoids set at 30 % probability, hydrogen atoms removed for clarity).

Table 1. Structural properties of **CoX** with X = I, Br, Cl.

	CoCl[a]	**CoBr**	**CoI**
Co—S1	2.1957(5)	2.1898(10)	2.178(3)
Co—S2	2.2056(5)	2.1984(9)	2.187(3)
Co—N1	1.9915(14)	1.993(3)	1.984(8)
Co—N2	2.0267(14)	2.022(3)	2.016(8)
Co—X	2.3336(5)	2.4888(7)	2.6938(18)
S1-Co-S2	78.427(19)	78.60(4)	78.91(12)
S1-Co-N1	92.57(5)	93.01(9)	93.9(3)
S1-Co-N2	142.15(4)	143.48(9)	145.7(3)
S2-Co-N1	163.72(5)	164.65(9)	165.6(3)
S2-Co-N2	97.73(4)	98.14(8)	98.2(3)
N1-Co-N2	80.99(6)	80.88(11)	80.6(4)
S1-Co-X	118.80(2)	118.34(3)	118.41(10)
S2-Co-X	104.64(2)	103.25(3)	101.86(10)
N1-Co-X	91.57(4)	92.03(8)	92.5(2)
N2-Co-X	98.73(4)	97.93(9)	95.7(3)

[a] Data taken from Ref. [25].

axial position. The Co^{III} ion is shifted approximately by 0.485 Å, 0.464 Å, and 0.435 Å from the mean equatorial plane (formed by N2S2) toward the axial halide ligand in **CoCl**, **CoBr**, and **CoI**, respectively. The equatorial Co—N and Co—S bond lengths are not sensitive to the nature of the halide (less than 3.5 pm difference), whereas the Co—X distance increases significantly from **CoCl** to **CoI** (2.3336(5) Å, 2.4888(7) Å, and 2.6938(18) Å,

respectively). The Co—S and Co—N bond lengths in all the complexes are slightly shorter than those in **Co₂SS²⁺**, which is consistent with the difference in the ionic radii of Co^{II} and Co^{III}. The valence angles of the equatorial plane evidence noticeable distortions in the plane, as attested by the S1-Co-N2 and S2-Co-N1 angles of 142.15(4)° and 163.72(5)° in **CoCl**, 143.48(9)° and 164.65(9)° in **CoBr**, and 145.7(3)° and 165.6(3)° in **CoI**.

From these two angles, the index of the degree of trigonality of a pentacoordinated geometry can be determined: $\tau_5 = (\beta - \alpha)/60$, in which α and β are the greatest two basal angles and $\alpha < \beta$. For a perfectly tetragonal pyramidal geometry, τ_5 is equal to zero, whereas it becomes equal to one for a perfectly trigonal-bipyramidal geometry.[26] The τ_5 values are 0.360, 0.353, and 0.332 for **CoCl**, **CoBr**, and **CoI**, respectively, in agreement with a distorted square pyramidal geometry in all cases.

Electronic absorption properties

The UV/Vis absorption spectra of the three complexes recorded in CH₂Cl₂ display three main transitions in the ranges 477–493 nm (1), 675–718 nm (2), and 804–857 nm (3) (Figure 2 and Table 2). Both the energy and intensity of these features are sensitive to the nature of the axial halide in a similar manner. Whereas their intensity increases from the chloride to the iodide derivative, their respective energy decreases. In particu-
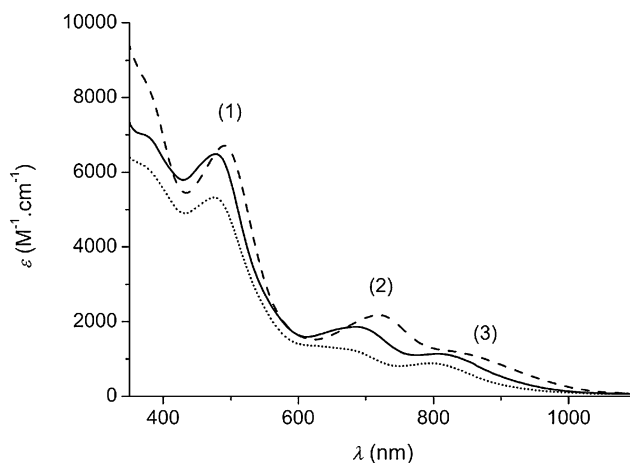

Figure 2. UV/Vis spectra of **CoBr** (solid line) and **CoI** (dashed line), compared with that of **CoCl** (dotted line). (0.19 mM solutions in CH₂Cl₂, 1 cm path length, 20 °C, aerobic conditions).

Table 2. Experimental (left) and TD-DFT calculated (right) UV/Vis absorption properties of **CoX** with X = I, Br, Cl in CH₂Cl₂.

	λ_{exptl} [nm] (ε_{exptl} [M⁻¹cm⁻¹])			λ_{calcd} [nm] (f_{calcd})		
CoCl[a]	477 (5318)[a]	675 (1250)[a]	804 (875)[a]	472 (0.056)	690 (0.026)	760 (0.009)
CoBr	486 (6400)	688 (1860)	814 (1135)	489 (0.050)	710 (0.034)	798 (0.004)
CoI	493 (6800)	718 (2250)	857 (1140)	508 (0.024)	741 (0.019)	862 (0.008)

[a] Data taken from Ref. [25].

lar, the energies of transitions (2) and (3) are noticeably more affected by the nature of the halide than that of (1). TD-DFT calculations were performed to determine the nature of these transitions. A good agreement between the calculated and experimental data was found, and the observed tendencies were reproduced well. The two high-energy transitions (1 and 2) are attributed to ligand-to-metal charge transfer (LMCT) transitions, whereas the lower-energy features (3) are associated with a mixed d–d/intraligand charge transfer (ILCT) transition. These latter results clearly show the strong influence of the halide ligand on transition (3), with a larger contribution for the iodide with respect to the chloride or bromide (see Supporting Information).

Magnetic properties

The magnetic susceptibility of **CoBr** and **CoI** was measured as a function of temperature (1.8–300 K). The temperature dependence of the χT product for the two complexes is shown in Figure 3, together with that of **CoCl** for comparison. The room-temperature χT values for the three complexes are consistent with the expected values for $S = 1$ species (Table 3). The
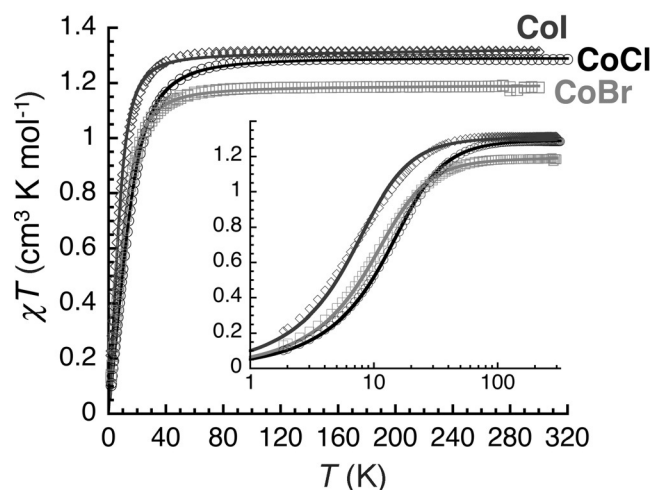

Figure 3. Temperature dependence of the χT product (χ is the molar magnetic susceptibility equal to M/H per cobalt complex) measured at 0.1 T for **CoCl** (○), **CoBr** (□) and **CoI** (◇). The solid lines are the best fits of the experimental data to the models described in the text. Inset: Expansion of the low-temperature region ($T < 100$ K).

magnetic susceptibility for all complexes remains constant down to approximately 30–50 K, consistent with magnetically isolated Co^{III} centers. At lower temperatures, the χT values display a notable decrease, explained by the presence of large ZFS. Considering the clear separation of the Co^{III} complexes in the crystal structure, and thus, the absence of obvious intermolecular magnetic interactions, a simple spin Hamiltonian including D and the isotropic Zeeman interaction (g) is considered to fit the experimental data with Equation (1) (Table 3).

$$\mathbf{H} = DS_z^{\,2} + g\mu_B\mu_0 HS \tag{1}$$

Together with g factors significantly larger than 2 [2.27(5), 2.17(5), and 2.28(5)], large positive D values of 35(1) cm^{-1}, 26(1) cm^{-1}, and 18(1) cm^{-1} are found for **CoCl**, **CoBr**, and **CoI** respectively. The decrease in D values from the chloride to the iodide derivative is unexpected, and theoretical calculations were performed to rationalize this observation (vide infra). The large g values found for **CoCl**, **CoBr**, and **CoI** evidence important spin-orbit contributions to the spin-only value, consistent with the notable magnetic anisotropy in the complexes.

The magnetic properties of the complexes were also studied in solution. The ^{1}H NMR spectra of both **CoBr** and **CoI** are consistent with paramagnetic species (Supporting Information). The effective magnetic moments determined in DMF solutions by the Evans method show that the triplet state is conserved in solution for both complexes (Table 3). This also confirms that the mononuclear structures of **CoBr** and **CoI** are retained in solution as for **CoCl**.

Quantum chemical calculations

Calculations were performed on optimized structures initiated from the respective X-ray data of the three complexes (Supporting Information). The optimized structures are very close to the experimental ones, with a maximum difference of 5 pm in the metal–ligand bond lengths.

Prediction of the spin state

DFT calculations were performed to determine the ground spin state of the complexes, as well as the stability of the first excit-

Table 3. Experimental determination of the spin states for **CoX** with X = I, Br, Cl.

	CoCl[a]	**CoBr**	**CoI**
Powder			
χT [cm^3 K mol^{-1}]	1.35	1.18	1.31
S	1	1	1
Solution			
μ_{eff} (μ_B) at 20 °C	2.44	2.63	2.94
χT [cm^3 K mol^{-1}]	0.74	0.86	1.07
S	1	1	1
[a] Data from Ref. [25].			

Table 4. Calculated Gibbs free energies for the singlet, triplet, and quintet states of **CoX** with X = I, Br, Cl at 0 K.

	Spin state	E [Eh]	Stability [kcal mol^{-1}]	Favored species
CoCl	$S = 0$	−4213.839378	+13.7	
	$S = 1$	−4213.861225	0	$S = 1 > S = 2 > S = 0$
	$S = 2$	−4213.847693	+8.5	
CoBr	$S = 0$	−6328.885087	+14.0	
	$S = 1$	−6328.907428	0	$S = 1 > S = 2 > S = 0$
	$S = 2$	−6328.890987	+10.3	
CoI	$S = 0$	−10675.294858	+8.5	
	$S = 1$	−10675.308411	0	$S = 1 > S = 0 > S = 2$
	$S = 2$	−10675.290705	+11.1	

ed spin states with respect to the ground state (Table 4). In all the complexes, a triplet ground spin state is predicted, in agreement with the experimental data. In the cases of **CoCl** and **CoBr**, the first excited spin state is $S = 2$ with the energy gap from the triplet state increasing from 8.5 to 10.3 kcal mol^{-1}, respectively. Conversely, for **CoI**, the first excited spin state is $S = 0$, with an energy gap of 8.5 kcal mol^{-1} with respect to the $S = 1$ ground state. The nature of the halide ligand thus notably affects the spin state energy spectrum with expected consequences on the ZFS (vide infra).

Electronic structure

Before calculation of the ZFS parameters, the electronic structures of the three complexes were investigated to help rationalize the results. This study was based on the set of quasi-restricted orbitals (QROs), as this approach has been previously applied with success (Figure 4).[9c, 12a, 27] In particular, we defined
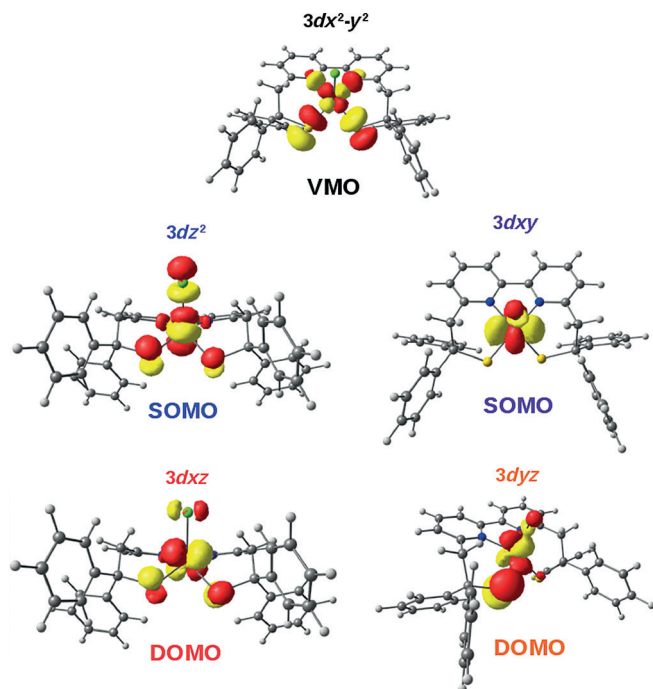

Figure 5. Energy diagram of the five 3d-orbitals of **CoX** with X = I, Br, Cl.

Figure 4. Graphical representation of the five 3d orbitals of **CoX** with X = Cl.

the energy diagram of the five 3d metal-based MOs of the three complexes. These square pyramidal complexes present the typical scheme of a pseudo C_{4V} symmetry, which corresponds to the loss of an axial ligand if starting from the O_h symmetry. In an octahedral coordination geometry, the two d_{z^2} and $d_{x^2-y^2}$ orbitals (e_g block) are degenerate and higher in energy than the set of d_{xy}, d_{xz}, and d_{yz} orbitals (t_{2g} block). Although going from O_h to C_{4V} symmetry does not affect the energy of $d_{x^2-y^2}$ and d_{xy} orbitals, it leads to a strong stabilization of the d_{z^2}, d_{xz}, and d_{yz} orbitals, consistently with the energy diagram shown in Figure 5. With respect to the $d_{x^2-y^2}$ orbital, the unoccupied virtual molecular orbital (VMO), the
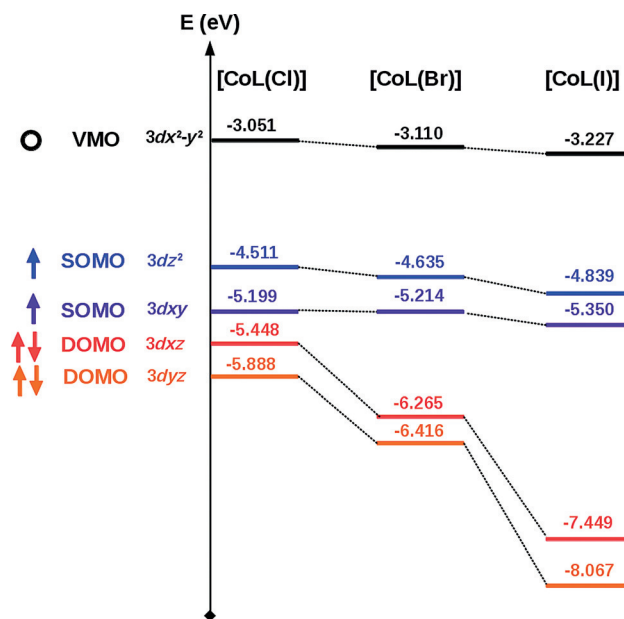
other four 3d metal-based orbitals are close in energy in **CoCl**, whereas in **CoI** the two singly occupied molecular orbitals (SOMOs), d_{z^2} and d_{xy}, are well separated from the two doubly occupied molecular orbitals (DOMOs), d_{xz} and d_{yz}. The much larger energy splitting between the DOMOs and the VMO in **CoI** than in **CoCl** (4.222 vs. 2.397 eV, Figure 5) disfavors transitions to $S = 2$ excited states. This is in coherence with a singlet as the first excited spin state for **CoI** (large energy gap) and a quintet for **CoCl** (smaller energy gap).

From Figure 5, it is also clear that the energy splitting between the SOMOs and DOMOs is dictated mainly by the varying degrees of stabilization of the DOMOs. Consistently with the structural properties of the complexes, the more distorted the square pyramidal geometry, the less stabilized are the d_{xz} and d_{yz} orbitals ($\tau_5 = 0.360$, 0.353, and 0.332, and metal shift out of the mean equatorial plane of 0.485, 0.464, and 0.435 Å for **CoCl**, **CoBr**, and **CoI**, respectively). Besides, it can be observed that both DOMOs have a main metal character in **CoI**, whereas they become notably delocalized over the halide ligand in **CoBr** and to a greater extent in **CoCl** (Supporting Information). The larger delocalization of the electronic density on the chloride observed for the DOMOs in **CoCl** with respect to **CoI** suggests that the covalency of the Co—halide bond depends on the nature of the halide, with Co—Cl more covalent than Co—I. This is fully supported by the Mülliken analysis, which shows an increase in the spin population found at the metal ion on going from the chloride (1.89) to the iodide (1.93) derivative.

Prediction of the ZFS

To the best of our knowledge, theoretical determination of the magnetic anisotropy of a clearly identified intermediate $S = 1$ Co^{III} ion has never been reported. Calculations have only

been performed in the case of a square planar $S=1$ cobalt complex containing two aromatic dithiolate ligands, as reported by the group of Wieghardt, and for which the authors cannot discriminate between a Co^{III} and a Co^{II}-radical species.[28] In the present case, the (+III) oxidation state of the cobalt ion could not be called into question, as evidenced by the above Mülliken analysis. The difference between the compounds arises from the nature of the thiolate ligands, that is, alkyl versus aromatic. Aromatic thiolate radical-based species can be strongly stabilized, whereas this is not the case for alkyl thiolates. With the present alkyl dithiolate L ligand and derivatives, Ni complexes have been isolated and characterized from the (+III) to (+I) oxidation states.[29] Conversely, it has been shown recently with Ni^{II} complexes containing one aromatic and one alkyl thiolate ligand that the one-electron reduction and oxidation processes occur mainly on the aromatic thiolate ligand, showing the difference in reactivity between these types of ligands.[30]

The ZFS parameters of the present three Co^{III} halide complexes have been predicted within the DFT framework, and

Figure 6. Individual contributions to the DFT-calculated ZFS parameters of **CoX** with X=I, Br, Cl.

Table 5. Experimental versus DFT- and CASSCF-calculated D values and their individual contributions for **CoX** with X=I, Br, Cl.

	CoCl	CoBr	CoI	CoCl(I)[b]
	Experimental			
g	2.27(5)[a]	2.17(5)	2.28(5)	
D_{exptl} [cm^{-1}]	+35(1)[a]	+26(1)	+18(1)	
	DFT calculated			
D_{calcd} [cm^{-1}]	+32.49	+27.23	+17.17	+24.62
D_{SSC} [cm^{-1}]	+0.94	+0.75	+0.63	+0.91
D_{SOC} [cm^{-1}]	+31.56	+26.48	+16.50	+23.79
D_{SOC} ($\alpha\alpha$) [cm^{-1}]	+11.63	+4.01	−0.30	+3.69
D_{SOC} ($\beta\beta$) [cm^{-1}]	+21.80	+10.38	−4.29	+10.86
D_{SOC} ($\alpha\beta$) [cm^{-1}]	−3.01	+12.63	+21.37	+9.04
D_{SOC} ($\beta\alpha$) [cm^{-1}]	+1.15	−0.53	−0.27	+0.17
	CASSCF calculated			
D_{calcd} [cm^{-1}]	+31.64	+21.98	+16.27	
D_{SSC} [cm^{-1}]	+0.59	−0.72	+2.21	
D_{SOC} [cm^{-1}]	+31.37	+21.98	+13.93	
$D_{S=1}$ [cm^{-1}]	+33.94	+13.70	−2.49	
$D_{S=0}$ [cm^{-1}]	−2.57	+8.28	+16.42	

[a] Data issued from Ref. [22]. [b] **CoCl(I)** is a theoretical complex corresponding to the optimized structure of **CoI**, in which the iodide has been replaced by chloride.

the results are reported in Table 5 and Figure 6. The agreement between the experimental and theoretical data is remarkable for DFT in both the sign and magnitude of D for all the complexes. The contribution of the spin–spin dipolar interaction is rather small (below 5% of the total contribution) and is approximately the same magnitude in all complexes (in the range 0.63–0.94 cm^{-1}). Regarding the different contributions to D_{SOC}, three main types of transitions are involved, that is, the two types of spin-conserving excitations from i) the DOMOs to the SOMOs ($\beta\beta$) and ii) the SOMOs to the VMO ($\alpha\alpha$), as well as iii) the spin-flip excitations between the two SOMOs ($\alpha\beta$). The values of each of these contributions to D_{SOC} evolve steadily as a function of the nature of the halide anion from the chloride
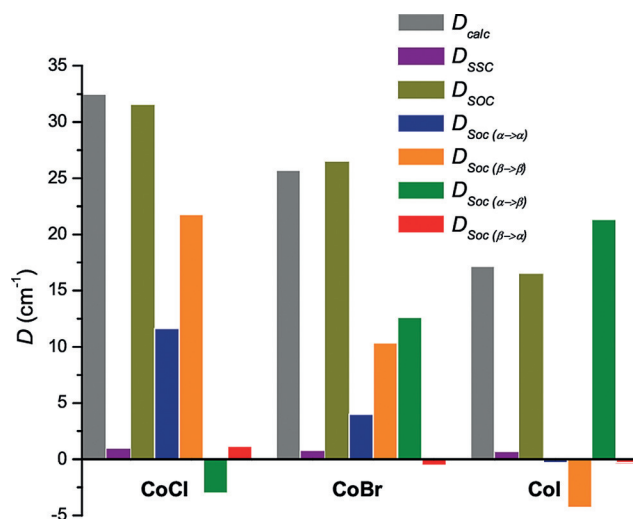
to the iodide, with inverse trends for the spin-flip $\alpha\beta$ (e.g. $D^{Cl}\alpha\rightarrow\beta < D^{Br}\alpha\rightarrow\beta < D^{I}\alpha\rightarrow\beta$) and spin-conserving $\beta\beta$ (e.g. $D^{Cl}\beta\rightarrow\beta > D^{Br}\beta\rightarrow\beta > D^{I}\beta\rightarrow\beta$) and to a lesser extent $\alpha\alpha$ excitations. Therefore, whereas the $\alpha\beta$ transitions are a main contribution to D_{SOC} in **CoI**, they become negligible for **CoCl**, for which the main contributions to D_{SOC} arise from both spin-conserving excitations. The **CoBr** complex represents an intermediate case.

To check the reliability of the above results, we performed ab initio calculations using the CASSCF approach (Table 5). The CASSCF-computed parameters compare well with those obtained by DFT. Indeed, both the CASSCF-calculated triplet ($D_{S=1}$) and singlet ($D_{S=0}$) contributions, which are related to the spin-conserving and spin-flip excitations, respectively, are consistent with the DFT calculation results. In the case of **CoCl**, the main contribution to D_{SOC} arises from the triplet states, whereas for **CoI** it originates from the singlet states. Consequently, it can be concluded that both CASSCF and DFT methods are appropriate for predicting the ZFS parameters of these intermediate spin Co^{III} halide complexes.

In an attempt to rationalize further the origin of the discrepancy in D between the three complexes, especially the impact of structural effects on D_{SOC} with respect to the nature of the halide, we performed DFT calculations on a theoretical complex. This corresponds to the optimized structure of **CoI**, in which the iodide ligand is replaced by chloride without any further optimization procedure. The resulting D value ($D_{calc}^{(I)Cl}$) of +24.63 cm^{-1} is between D_{calc}^{Cl} and D_{calc}^{I} (+32.49 and +17.17 cm^{-1}, respectively), with all contributions to D following the same tendency (Table 5). The increase from $D_{calc}^{(I)Cl}$ to D_{calc}^{Cl} implies the intrinsic effect of the structure on the D_{SOC} contribution, whereas the increase from D_{calc}^{I} to $D_{calc}^{(I)Cl}$ shows that of the nature of the halide.

Conclusion

A series of mononuclear pentacoordinated halide Co^{III} complexes displaying an intermediate $S = 1$ spin state has been investigated. It has been shown experimentally that the magnetic anisotropy of these complexes is sensitive to the nature of the halide, but in an unexpected way: the largest D value was measured for the chloride compound and the smallest for the iodide one. To the best of our knowledge, examples of such reported behavior are still limited to: 1) two $S = 2$ pseudo-tetrahedral Co^I complexes, in which the D value decreases from $+6.00$ to $+3.89$ cm^{-1} from the chloride to the bromide derivative;[10b] 2) an $S = 2$ Mn^{III} iodide complex that displays an unexpected small positive D value of $+0.604$ cm^{-1} in an elongated octahedral environment;[31] and 3) a series of $S = 1$ pseudo-tetrahedral Ni^{II} complexes, in which D goes from $+3.9$ to -22.8 cm^{-1} from the chloride to the iodide derivative.[10a, 13b] Conversely, in most previous studies, it has been observed that the magnitude of D increases from the chloride to the iodide metal complexes.[12b, 16] This previously reported trend was tentatively correlated with the magnitude of the SOC contribution of the halide, which can override the SOC contribution of the metal ion center. However, using theoretical Mn^{II},[12b] and Fe^{III},[32] models, it was also demonstrated that the main contribution to the final D values results from a balance between the metal ion and halide SOC contributions, which are proportional to the $\xi_{Mn}\xi_X$ product, ($\xi_{Mn/X}$ is the metal ion/ligand SOC constant). Therefore, depending on the metal ion and the halide, the SOC contribution of the heavier ligand and the metal ion can compensate each other, leading to an inverse tendency, as found in the present case.

At a further level of analysis, we have been able to define a magnetostructural correlation. **CoCl** displays the more distorted square pyramidal geometry within the series (higher τ_5 parameter and larger metal displacement out of the equatorial plane), leading to destabilization of the DOMOs and a smaller energy gap with the VMOs, which explains the accessibility of a quintet as the first excited state. Coherently, in the more distorted **CoCl** complex, the SOMOs–DOMOs energy gap becomes smaller, favoring the spin-conserving excitations that contribute mainly to the ZFS parameters of **CoCl**. In contrast, **CoI** presents the least distorted geometry and the most energetically stabilized DOMOs, such that the main contribution to D_{SOC} arises from spin-flip excitations ($\alpha\beta$) and the first excited spin state is a singlet. In any case, other contributing factors to D should be taken into account, including the SOC contribution of the ligands and the covalency of the Co—halide bond. However, it is difficult to identify the weight of each of these factors; the overall data demonstrate that all of them affect the final D values in a balanced manner.

Finally, this investigation shows that both DFT and CASSCF are powerful tools for the prediction of both the sign and magnitude of D for $S = 1$ Co^{III} complexes. However, it should be noted that DFT is the most appropriate method for determining the different contributions to D, which is particularly useful for obtaining structure–property relationships. It also remains clear that no general rule can be extrapolated from the present case: for each metal ion, at each oxidation and spin state, benchmark investigations are required to define magnetostructural correlations and to establish the most appropriate theoretical method to predict the ZFS parameters, rendering the rational synthesis of SMMs based on a single metal ion still very challenging.

Experimental Section

Co_2SS^{2+} was prepared according to a reported procedure.[25] All reagents and solvents were used as received. ^1H NMR spectra were recorded on a Bruker Avance III 400 MHz spectrometer using standard Bruker pulse sequences. Chemical shifts are reported in ppm referenced to residual solvent protons (d_7-DMF). The infrared spectra were recorded on a Magna-IR TM 550 Nicolet spectrometer as KBr pellets. The electronic absorption spectra were recorded on a Varian Cary 300 absorption spectrophotometer in quartz cells (optical path length: 1 cm). The ESI-MS experiments were performed with a Bruker Esquire 3000 Plus ion trap spectrometer equipped with an electrospray ion (ESI) source. The samples were analyzed in positive and negative ionization mode by direct perfusion in the ESI-MS interface (ESI capillary voltage = 2 kV, sampling cone voltage = 40 V).

Synthesis of [Co^{III}L(X)](CoX, X = Br or I)

Solid tetrabutylammonium bromide (303 mg, 0.940 mmol) or tetrabutylammonium iodide (347 mg, 0.940 mmol) was added to a solution of **Co$_2$SS**(PF$_6$)$_2$ (96 mg, 0.060 mmol) in CH$_2$Cl$_2$ (10 mL). After stirring for 15 min, the solvent was removed under vacuum. The dark brown residue was washed with acetonitrile (3×10 mL), dried, and collected.

CoBr (60 mg, 0.084 mmol, 70% yield). IR: $\tilde{\nu} = 3052$ (m), 3027 (w), 1958 (w), 1890 (w), 1809 (w), 1602 (s), 1570 (s), 1488 (s), 1469 (m), 1443 (s), 1266 (w), 1184 (w), 1157 (w), 1126 (m), 1084 (m), 1060 (m), 1034 (m), 793 (m), 754 (m), 747 (m), 697 (vs), 534 (m), 522 cm^{-1} (m); ^1H NMR (400 MHz, CD$_2$Cl$_2$): $\delta = -16.20$, -11.36, -10.66, -4.19, 7.39, 7.55, 11.91, 12.12, 12.36, 26.13, 28.27 ppm; ESI-MS (5×10^{-5} M, CH$_3$CN, m/z, I%): 637.2, 77 [CoL]$^+$; 757.1, 56 [CoLBr·MeCN]$^+$; 1355.2, 100 [Co$_2$L$_2$Br]$^+$ 1473.1, 90 [Co$_2$L$_2$Br$_2$·MeCN]$^+$ (positive ion mode); 797.1, 37 [CoLBr$_2$]$^-$; 1513.4, 100 [Co$_2$L$_2$Br$_3$]$^-$ (negative ion mode); absorption spectrum in CH$_2$Cl$_2$: λ_{max} (ε) = 822 (≈ 1100), 683 (≈ 1900), 475 (≈ 6400), 380 nm (≈ 6900 M^{-1}cm^{-1}).

CoI (77 mg, 0.101 mmol, 84%). IR: $\tilde{\nu} = 3052$ (m), 3027 (w), 1958 (w), 1890 (w), 1809 (w), 1602 (s), 1570 (s), 1488 (s), 1469 (m), 1443 (s), 1266 (w), 1184 (w), 1157 (w), 1126 (m), 1084 (m), 1060 (m), 1034 (vs), 793 (m), 754 (m), 747 (m), 697 cm^{-1} (vs); ^1H NMR (400 MHz, CD$_2$Cl$_2$): $\delta = -22.51$, -16.21, -11.35, -4.20, -3.72, 7.37, 7.55, 11.90, 12.11, 12.36, 22.88, 26.12, 28.25 ppm; ESI-MS (5×10^{-5} M, CH$_3$CN, m/z, I%): 637.2, 100 [CoL]$^+$; 1401.2, 50 [Co$_2$L$_2$I]$^+$ (positive ion mode); 891.0, 16 [CoLI$_2$]$^-$; 1655.2, 100 [Co$_2$L$_2$I$_3$]$^-$ (negative ion mode); absorption spectrum in CH$_2$Cl$_2$: λ_{max} (ε) = 859 (≈ 1200), 726 (≈ 2200), 490 (≈ 6800), 377 nm (≈ 8200 M^{-1}cm^{-1}).

X-ray-suitable dark brown single crystals of **CoX** (X = Br, I) were obtained by slow evaporation of a solution of the corresponding complex in toluene/CH$_2$Cl$_2$ (1:1).

Magnetic measurements

The magnetic susceptibility measurements performed on powdered samples were obtained with an MPMS-XL Quantum Design SQUID magnetometer. This magnetometer works between 1.8 and

400 K for dc applied fields ranging from −7 to 7 T. Measurements were performed on polycrystalline samples of 10.8 and 15.6 mg for **CoBr** and **CoI**, respectively, introduced in a polyethylene bag (3× 0.5×0.02 cm; ≈30 mg) and covered with mineral oil (typically 8– 10 mg). The ac susceptibility measurements were measured with an oscillating ac field of 3 Oe with a frequency between 1 and 1500 Hz. It is worth noting that no out-of-phase ac susceptibility signal was detected above 1.8 K in zero dc field. The magnetic data were corrected for the sample holder (plastic bag) and the di-amagnetic contribution. Magnetic susceptibility measurements on solution samples were performed following Evans' method[33] using precision-made coaxial tubes. Cyclohexane (5% by volume) was used as the internal standard in CD_2Cl_2. Molar susceptibilities were calculated according to Equation (2), in which χ_0 is the mass susceptibility of the pure solvent (cgs units), $\Delta\nu$ is the paramagnetic shift (Hz), ν_0 is the operating RF frequency of the spectrometer (Hz), c is the concentration (mol L^{-1}) of the paramagnetic molecule, and M is its molecular weight.

$$\chi \approx M \left(\chi_0 + 3000\Delta\nu/4\pi\nu_0 cM \right) \qquad (2)$$

The values were corrected for the ligand diamagnetic susceptibility derived from Pascal's constants, giving χ^{corr}. The magnetic moments (μ_{eff}) were then calculated according to Equation (3).

$$\mu_{eff} = (8 \times \chi T)^{1/2}, \text{ in which } T = 293 \text{ K} \qquad (3)$$

Computational details

All theoretical calculations were performed with the ORCA program package.[34] Full geometry optimizations were undertaken for all complexes using the GGA functional BP86[35] in combination with the TZV/P[36] basis set for all atoms, and by taking advantage of the resolution of the identity (RI) approximation in the Split-RI-J variant[37] with the appropriate Coulomb fitting sets.[38] Increased integration grids (Grid4 in ORCA convention) and tight SCF convergence criteria were used. Additional corrections including dispersion, solvation, and relativistic effects were also considered in benchmark calculations. In all cases, the optimized geometries resulted in structures with similar deviations from the experimental data (see Supporting Information). Electronic structures and Molecular Orbital diagrams were obtained from relativistic single-point calculations using the hybrid functional B3LYP[39] together with the TZV/P[36] basis set. Scalar relativistic effects were included by using the scalar relativistic zero-order regular approximation (ZORA)[40] and the scalar relativistically recontracted (SARC)[41] version of the def2-TZVP(-f) basis set[42] together with the decontracted def2-TZVP/J Coulomb fitting basis sets for all atoms. Increased integration grids (Grid4 and GridX4 in ORCA convention) and tight SCF convergence criteria were used in the calculations. The relative energies were computed from the gas-phase optimized structures as a sum of electronic energy, relativistic and thermal corrections to the free energy. Optical properties were predicted from additional single-point calculations using the hybrid functional B3LYP[39] together with the TZV/P[36] basis set. For that purpose, solvent effects were accounted and we used the CH_2Cl_2 ($\varepsilon = 9.08$) solvent within the framework of the conductor-like screening (COSMO) dielectric continuum approach.[43] Electronic transition energies and dipole moments for all models were calculated using time-dependent

DFT (TD-DFT)[44] within the Tamm–Dancoff approximation.[45] To increase computational efficiency, the RI approximation[46] was used in calculating the Coulomb term, and at least 30 excited states were calculated in each case. For each transition, difference density plots were generated using the orca plot utility program and were visualized with the Chemcraft program.[47] Zero Field Splitting (ZFS) parameters were obtained from relativistic single-point calculations using the hybrid functional B3LYP[39] and the scalar relativistic zero-order regular approximation (ZORA).[40] Direct spin–spin (SSC) and spin-orbit couplings (SOC) were taken into account. For the estimation of the SOC effects, the mean-field approximation (SOMF), including both the spin-own-orbit and spin-other-orbit interactions in the exchange term, as well as the coupled-perturbed (CP) approach, was used. The spin–spin contribution to the ZFS was calculated from the equation of McWeeny and Mizuno,[48] in which the spin density matrix is obtained on the basis of the spin-unrestricted natural orbital (UNO) determinant.[49] ZFS parameters were alternatively obtained from ab initio calculations based on the complete active space self-consistent field (CASSCF) approach. The spin-orbit coupling was calculated within a quasi-degenerate perturbation theory formalism, in which the SOC operator is diagonalized in a basis of multiconfigurational wavefunctions obtained from a full configuration interaction (CI) calculation in a limited set of active electrons and orbitals obtained from a preceding CASSCF calculation.[28] The active space was chosen to consist of six active electrons occupying the five 3d-based molecular orbitals CAS(6,5). The SOC matrix was diagonalized on the basis of all possible triplet (35) and singlet (45) states. The spin–spin (SSC) contribution to the ZFS was calculated on the basis of the single root CASSCF (12,7) wavefunction.[50]

[1] a) R. J. Blagg, C. A. Muryn, E. J. L. McInnes, F. Tuna, R. E. P. Winpenny, *Angew. Chem. Int. Ed.* **2011**, *50*, 6530–6533; *Angew. Chem.* **2011**, *123*, 6660–6663; b) K. R. Meihaus, J. R. Long, *J. Am. Chem. Soc.* **2013**, *135*, 17952–17957; c) L. Ungur, J. J. Le Roy, I. Korobkov, M. Murugesu, L. F. Chibotaru, *Angew. Chem. Int. Ed.* **2014**, *53*, 4413–4417; *Angew. Chem.* **2014**, *126*, 4502–4506; d) J. J. Le Roy, L. Ungur, I. Korobkov, L. F. Chibotaru, M. Murugesu, *J. Am. Chem. Soc.* **2014**, *136*, 8003–8010.

[2] a) G. A. Craig, M. Murrie, *Chem. Soc. Rev.* **2015**, *44*, 2135–2147; b) M. Atanasov, D. Aravena, E. Suturina, E. Bill, D. Maganas, F. Neese, *Coord. Chem. Rev.* **2015**, *289–290*, 177–214; c) S. Gomez-Coca, D. Aravena, R. Morales, E. Ruiz, *Coord. Chem. Rev.* **2015**, *289*, 379–392.

[3] a) K. S. Pedersen, M. Sigrist, M. A. Sorensen, A. L. Barra, T. Weyhermuller, S. Piligkos, C. A. Thuesen, M. G. Vinum, H. Mutka, H. Weihe, R. Clérac, J. Bendix, *Angew. Chem. Int. Ed.* **2014**, *53*, 1351–1354; *Angew. Chem.* **2014**, *126*, 1375–1378; b) J. Martínez-Lillo, J. Faus, F. Lloret, M. Julve, *Coord. Chem. Rev.* **2015**, *289–290*, 215–237.

[4] M. Gruden-Pavlovic, M. Peric, M. Zlatar, P. Garcia-Fernandez, *Chem. Sci.* **2014**, *5*, 1453–1462.

[5] K. Marriott, L. Bhaskaran, C. Wilson, M. Medarde, S. T. Ochsenbein, S. Hill, M. Murrie, *Chem. Sci.* **2015**, *6*, 6823–6828.

[6] J. Vallejo, I. Castro, R. Ruiz-García, J. Cano, M. Julve, F. Lloret, G. De Munno, W. Wernsdorfer, E. Pardo, *J. Am. Chem. Soc.* **2012**, *134*, 15704–15707.

[7] J. Krzystek, A. Ozarowski, J. Telser, *Coord. Chem. Rev.* **2006**, *250*, 2308–2324.

[8] R. Boca, *Coord. Chem. Rev.* **2004**, *248*, 757–815.

[9] a) R. Reviakine, A. V. Arbuznikov, J.-C. Tremblay, C. Remenyi, O. L. Malkina, V. G. Malkin, M. Kaupp, *J. Chem. Phys.* **2006**, *125*, 054110; b) S. Zein, C. Duboc, W. Lubitz, F. Neese, *Inorg. Chem.* **2008**, *47*, 134–142; c) C. Duboc, M. N. Collomb, F. Neese, *Appl. Magn. Reson.* **2010**, *37*, 229–245; d) C. Duboc, D. Ganyushin, K. Sivalingam, M.-N. Collomb, F. Neese, *J. Phys. Chem. A* **2010**, *114*, 10750–10758.

[10] a) S. Ye, F. Neese, *J. Chem. Theory Comput.* **2012**, *8*, 2344–2351; b) J. Krzystek, A. Ozarowski, S. A. Zvyagin, J. Telser, *Inorg. Chem.* **2012**, *51*, 4954–4964; c) F. Neese in Calculation of EPR and NMR Parameters Theory and Applications (Eds.: M. Kaupp, M. Bühl, V. G. Malkin), Wiley-VCH, Weinheim, **2004**.

[11] a) S. K. Singh, T. Gupta, P. Badkur, G. Rajaraman, *Chem. Eur. J.* **2014**, *20*, 10305–10313; b) S. Ye, F. Neese, A. Ozarowski, D. Smirnov, J. Krzystek, J. Telser, J.-H. Liao, C.-H. Hung, W.-C. Chu, Y.-F. Tsai, R.-C. Wang, K.-Y. Chen, H.-F. Hsu, *Inorg. Chem.* **2010**, *49*, 977–988; c) J. Martinez-Lillo, T. F. Mastropietro, E. Lhotel, C. Paulsen, J. Cano, G. De Munno, J. Faus, F. Lloret, M. Julve, S. Nellutla, J. Krzystek, *J. Am. Chem. Soc.* **2013**, *135*, 13737–13748; d) A. Kubica, J. Kowalewski, D. Kruk, M. Odelius, *J. Chem. Phys.* **2013**, *138*, 0; e) R. Maurice, C. de Graaf, N. Guihery, *Phys. Chem. Chem. Phys.* **2013**, *15*, 18784–18804.

[12] a) C. Duboc, M. N. Collomb, J. Pécaut, A. Deronzier, F. Neese, *Chem. Eur. J.* **2008**, *14*, 6498–6509; b) C. Duboc, T. Phoeung, S. Zein, J. Pécaut, M. N. Collomb, F. Neese, *Inorg. Chem.* **2007**, *46*, 4905–4916.

[13] a) D. Schweinfurth, J. Krzystek, I. Schapiro, S. Demeshko, J. Klein, J. Telser, A. Ozarowski, C.-Y. Su, F. Meyer, M. Atanasov, F. Neese, B. Sarkar, *Inorg. Chem.* **2013**, *52*, 6880–6892; b) P. J. Desrochers, J. Telser, S. A. Zvyagin, A. Ozarowski, J. Krzystek, D. A. Vicic, *Inorg. Chem.* **2006**, *45*, 8930–8941; c) R. Maurice, R. Bastardis, C. de Graaf, N. Suaud, T. Mallah, N. Guihery, *J. Chem. Theory Comput.* **2009**, *5*, 2977–2984.

[14] M. Atanasov, D. Ganyushin, D. A. Pantazis, K. Sivalingam, F. Neese, *Inorg. Chem.* **2011**, *50*, 7460–7477.

[15] S. Vaidya, A. Upadhyay, S. K. Singh, T. Gupta, S. Tewary, S. K. Langley, J. P. S. Walsh, K. S. Murray, G. Rajaraman, M. Shanmugam, *Chem. Commun.* **2015**, *51*, 3739–3742.

[16] a) H. I. Karunadasa, K. D. Arquero, L. A. Berben, J. R. Long, *Inorg. Chem.* **2010**, *49*, 4738–4740; b) C. Mantel, C. Baffert, I. Romero, A. Deronzier, J. Pécaut, M. N. Collomb, C. Duboc, *Inorg. Chem.* **2004**, *43*, 6455–6463; c) M. R. Saber, K. R. Dunbar, *Chem. Commun.* **2014**, *50*, 12266–12269; d) J. Krzystek, S. A. Zvyagin, A. Ozarowski, A. T. Fiedler, T. C. Brunold, J. Telser, *J. Am. Chem. Soc.* **2004**, *126*, 2148–2155; e) F. Yang, Q. Zhou, Y. Zhang, G. Zeng, G. Li, Z. Shi, B. Wang, S. Feng, *Chem. Commun.* **2013**, *49*, 5289–5291; f) R. Boča, J. Miklovič, J. Titiš, *Inorg. Chem.* **2014**, *53*, 2367–2369.

[17] A. K. Bar, C. Pichon, J.-P. Sutter, *Coord. Chem. Rev.* **2015**, DOI: 10.1016/j.ccr.2015.06.013.

[18] R. J. Deeth, D. L. Foulis, B. J. Williams-Hubbard, *Dalton Trans.* **2003**, 3949–3955.

[19] J. Kozhukh, M. A. Minier, S. J. Lippard, *Inorg. Chem.* **2015**, *54*, 418–424.

[20] E. R. King, G. T. Sazama, T. A. Betley, *J. Am. Chem. Soc.* **2012**, *134*, 17858–17861.

[21] a) B. Ramdhanie, L. N. Zakharov, A. L. Rheingold, D. P. Goldberg, *Inorg. Chem.* **2002**, *41*, 4105–4107; b) S. Licoccia, R. Paolesse in *Metal Complexes of Corroles and other Corrinoids, Vol. 84*, Springer, Berlin, **1995**, pp. 71–133.

[22] a) S. E. Harnung, E. Larsen, *Inorg. Chem.* **2007**, *46*, 5166–5173; b) J. C. Brewer, T. J. Collins, M. R. Smith, B. D. Santarsiero, *J. Am. Chem. Soc.* **1988**, *110*, 423–428.

[23] a) M. A. García-Monforte, I. Ara, A. Martín, B. Menjón, M. Tomás, P. J. Alonso, A. B. Arauzo, J. I. Martínez, C. Rillo, *Inorg. Chem.* **2014**, *53*, 12384–12395; b) P. J. Van der Put, A. A. Schilperoord, *Inorg. Chem.* **1974**, *13*, 2476–2481; c) P. J. M. W. L. Birker, J. J. Bour, J. J. Steggerda, *Inorg. Chem.* **1973**, *12*, 1254–1259.

[24] C. H. Cho, T. Y. Chien, J. H. Chen, S. S. Wang, J. Y. Tung, *Dalton Trans.* **2010**, *39*, 2609–2614.

[25] M. Gennari, B. Gerey, N. Hall, J. Pécaut, M.-N. Collomb, M. Rouzières, R. Clérac, M. Orio, C. Duboc, *Angew. Chem. Int. Ed.* **2014**, *53*, 5318–5321; *Angew. Chem.* **2014**, *126*, 5422–5425.

[26] A. W. Addison, T. N. Rao, J. Reedijk, J. Vanrijn, G. C. Verschoor, *J. Chem. Soc. Dalton Trans.* **1984**, 1349–1356.

[27] J. C. Schöneboom, F. Neese, W. Thiel, *J. Am. Chem. Soc.* **2005**, *127*, 5840–5853.

[28] K. Ray, A. Begum, T. Weyhermuller, S. Piligkos, J. van Slageren, F. Neese, K. Wieghardt, *J. Am. Chem. Soc.* **2005**, *127*, 4403–4415.

[29] a) M. Gennari, M. Orio, J. Pécaut, E. Bothe, F. Neese, M.-N. Collomb, C. Duboc, *Inorg. Chem.* **2011**, *50*, 3707–3716; b) M. Gennari, M. Orio, J. Pécaut, F. Neese, M.-N. Collomb, C. Duboc, *Inorg. Chem.* **2010**, *49*, 6399–6401.

[30] E. P. Broering, S. Dillon, E. M. Gale, R. A. Steiner, J. Telser, T. C. Brunold, T. C. Harrop, *Inorg. Chem.* **2015**, *54*, 3815–3828.

[31] S. Mossin, H. Weihe, A. L. Barra, *J. Am. Chem. Soc.* **2002**, *124*, 8764–8765.

[32] F. Neese, E. I. Solomon, *Inorg. Chem.* **1998**, *37*, 6568–6582.

[33] a) D. F. Evans, *J. Chem. Soc.* **1959**, 2003–2005; b) S. K. Sur, *J. Magn. Reson.* **1989**, *82*, 169–173.

[34] F. Neese, *Wiley Interdiscip. Rev. Comput. Mol. Sci.* **2012**, *2*, 73–78.

[35] a) J. P. Perdew, *Phys. Rev. B* **1986**, *33*, 8822–8824; b) J. P. Perdew, *Phys. Rev. B* **1986**, *34*, 7406–7406; c) A. D. Becke, *Phys. Rev. A* **1988**, *38*, 3098–3100.

[36] A. Schäfer, C. Huber, R. Ahlrichs, *J. Chem. Phys.* **1994**, *100*, 5829–5835.

[37] F. Neese, *J. Comput. Chem.* **2003**, *24*, 1740–1747.

[38] F. Weigend, *Phys. Chem. Chem. Phys.* **2006**, *8*, 1057–1065.

[39] a) A. D. Becke, *J. Chem. Phys.* **1993**, *98*, 1372–1377; b) C. T. Lee, W. T. Yang, R. G. Parr, *Phys. Rev. B* **1988**, *37*, 785–789.

[40] C. van Wüllen, *J. Chem. Phys.* **1998**, *109*, 392–399.

[41] a) D. A. Pantazis, X. Y. Chen, C. R. Landis, F. Neese, *J. Chem. Theory Comput.* **2008**, *4*, 908–919; b) D. A. Pantazis, F. Neese, *J. Chem. Theory Comput.* **2009**, *5*, 2229–2238.

[42] F. Weigend, R. Ahlrichs, *Phys. Chem. Chem. Phys.* **2005**, *7*, 3297–3305.

[43] A. Klamt, G. Schürmann, *J. Chem. Soc. Perkin Trans. 2* **1993**, 799–805.

[44] a) M. E. Casida in Recent Advances in Density Functional Theory, Part I (Ed.: D. P. Chong), World Scientific, Singapore, **1995**; b) R. E. Stratmann, G. E. Scuseria, M. J. Frisch, *J. Chem. Phys.* **1998**, *109*, 8218–8224; c) R. Bauernschmitt, R. Ahlrichs, *Chem. Phys. Lett.* **1996**, *256*, 454–464.

[45] a) S. Hirata, M. Head-Gordon, *Chem. Phys. Lett.* **1999**, *314*, 291–299; b) S. Hirata, M. Head-Gordon, *Chem. Phys. Lett.* **1999**, *302*, 375–382.

[46] F. Neese, *J. Chem. Phys.* **2001**, *115*, 11080–11080.

[47] Chemcraft, http://chemcraftprog.com.

[48] R. McWeeny, Y. Mizuno, *Proc. R. Soc. London Ser. A* **1961**, *259*, 554–577.

[49] a) S. Sinnecker, F. Neese, *J. Phys. Chem. A* **2006**, *110*, 12267–12275; b) F. Neese, *J. Chem. Phys.* **2007**, *127*, 164112.

[50] D. Ganyushin, F. Neese, *J. Chem. Phys.* **2006**, *125*, 024103.